CrossMark

ARTICLE

Annealing optimization for tin–lead eutectic solder by constitutive experiment and simulation

Xu Long,[a] Shaobin Wang, Xu He, and Yao Yao[b]
School of Mechanics, Civil Engineering and Architecture, Northwestern Polytechnical University, Xi'an 710072, People's Republic of China

(Received 21 February 2017; accepted 10 April 2017)

For Sn–Pb eutectic solder alloy, uniaxial tensile tests were conducted to dog-bone type specimens annealed at different temperatures (60–180 °C) and durations (2–48 h). Low strain rates ranging from 10^{-4} s^{-1} to 10^{-3} s^{-1} were applied to study the competition between creep and plasticity and also the rate dependent effect of annealing condition. It is found that the influence of annealing temperature on material properties is more than that of annealing duration. Higher temperature up to 180 °C generally leads to higher yield and ultimate stresses and ultimate strain of annealed specimens. The optimal annealing condition is suggested to be 180 °C for 6 h for stable and efficient improvements in both strength and ductility. By proposing a concise unified creep and plasticity constitutive model, the sensitivity to strain rate and annealing condition is quantified with consideration of both creep and hardening properties. Parameter calibration theoretically confirms the observed optimal annealing condition in experiments.

I. INTRODUCTION

In the electrical and electronic equipments, electronic packaging interconnects are evolving to lead-free solder materials as legislated by the restriction of the use of certain hazardous substances (RoHS).[1] However, due to the outstanding solderability and reliability under complicated working conditions, tin–lead eutectic (63Sn–37Pb, wt%) solder materials are exempted from electrical and electronic equipments for military or extraterrestrial purpose[2] and thus are still widely applied in the defense and aerospace industries.

The tin whiskers that form on nonleaded solder, which can cause short circuits, other reliability problems, and deleterious effect on the reliability of space electronic system, is found due to the whisker growth.[3,4] The European Space Agency (ESA) contractual requirements for component, PCB, and assembly are all based on Sn–Pb technology to maintain a space quality widely assessed and qualified. So far, no replacement for the tin–lead or indium–lead solders used by ESA in ECSS-Q-ST-70-08C[5] and ECSS-1-ST-70-38C.[6]

In the past decades, a few design factors of solder materials concerning reliability have been investigated, such as creep resistance, shear strength, fracture propagation, soldering process parameters, microstructural evolution, and thermal cyclic fatigue life.[7–14] The tensile behavior of bulk solder material, which is one of the key parameters, is essential to facilitate numerical evaluations of mechanical resistance of solder bumps.[15,16] However, most of the experimental and theoretical studies on stress–strain relationships of solders did not consider the annealing effect.[17,18] Generally, it is assumed that residual stress from machining or thermal operations when obtaining the specimens should be released after routine annealing treatment.

This assumption leads to potential issues which may influence the mechanical behavior of solder materials and joints. Besides the annealing effect on solder joint behavior,[19,20] quite different annealing conditions (i.e., temperature and duration) for Sn–Pb eutectic solder have been applied as listed in Table I. Residual stress was assumed to be removed as default, and no explicit explanation was given for the underlying dominant mechanism. It has been found that the resulting experimental data is not consistent from different works in terms of the relationship between tensile behavior and strain rate. If different annealing durations and temperatures affect the tensile behavior, the experimental findings based on a specific annealing treatment are not generalized and cannot be adopted for the other conditions. The effect of annealing duration and temperature on the tensile property of Sn–Pb eutectic solder alloy plays a crucial role in practice.

To address the solder joint reliability performance in electronic assemblies, the annealing effect on intermetallic compounds have been thoroughly investigated. Even though annealing process is not commonly used for solder joint fabrication nowadays, a good number of experimental studies in the literature show that appropriate annealing treatment can improve the mechanical capacity of solder

Contributing Editor: Jürgen Eckert
Address all correspondence to these authors.
[a]e-mail: xulong@nwpu.edu.cn
[b]e-mail: yaoy@nwpu.edu.cn
DOI: 10.1557/jmr.2017.166

https://doi.org/10.1557/jmr.2017.166 Published online by Cambridge University Press

 © Materials Research Society 2017

TABLE I. Different annealing conditions and testing types for Sn–Pb eutectic solder specimens.[21–29]

Annealing condition		Testing condition		
Temperature (°C)	Duration (h)	Loading type and strain rate (s^{-1})	Temperature (°C)	Reference
40	2	Low-cycle fatigue	40	Chen et al.[26]
100	2	Tension 10^{-3}–10^{-1}	40, 80, 100, 125	Nose et al.[22]
100	1	Tension 1.67×10^{-4}–1.67×10^{-2}	−40, 20, 120	Shohji et al.[23]
100	1	Tension 1.67×10^{-4}–1.67×10^{-2}	25, 80, 120	Shohji et al.[24]
No annealing specified		Tension 7×10^{-5}–7×10^{-3}	25, 100, 140, 170	Kawashima et al.[21]
Step 1: 100 Step 2: 125	Step 1: 2 Step 2: 1	Tension 10^{-3}–10^{-1}	40, 80, 125	Zhang et al.[25]
150	10	Electro-contact heating	25	Chen and Yang[27]
150	10	Creep under current	50, 70, 90, 110	Chen and Yang[28]
150	10	Creep	30, 40, 50, 60, 70	Xuan et al.[29]

joints by further interfacial diffusion at the intermetallic compound layer. However, the annealing effect on the mechanical properties of Sn–Pb eutectic solder material is still left open. So the annealing effect for Sn–Pb solder joints in the aerospace industry is not well established. Without such a standard annealing treatment, the subsequent experimental study on the mechanical properties of solder alloy may not be consistent with each other. Therefore, the experimental findings based on different annealing treatments show lack of generality. On the other hand, a concise constitutive model is required by industry to perform efficient numerical analysis of solder joints based on the well calibrated annealing effect. These limitations as discussed above motivate the experimental and theoretical studies of the present paper.

In the present study, a wide range of temperatures and durations are applied as annealing treatment to remove the residual stress and expect to regain the homogenous microstructure with minimized free energy. In addition, the strain rates ranging from 10^{-4} s^{-1}–10^{-3} s^{-1} are applied to study its rate dependence on the tensile behavior of specimens annealed at different temperatures and durations. The optimized annealing condition and the applied strain rate to determine the saturation stress are suggested. To reveal the annealing effect to rate dependence and facilitate numerical simulations, a concise constitutive model for 63Sn–37Pb solder alloy is proposed based on the unified creep and plasticity theory. The effect of annealing condition is confirmed by correlating experimental and numerical results.

II. EXPERIMENTAL INVESTIGATION OF ANNEALING EFFECT ON TENSILE PROPERTY OF SN–PB EUTECTIC SOLDER

A. Experimental program

It is well accepted that the residual stress can be removed if sufficient annealing treatment is carried out. Thus, the annealing condition is concentrated in the present study to achieve a residual stress-free state after annealing treatment. In the experiment, the effect of cooling condition[30,31] can be neglected if sufficient annealing treatment is provided; otherwise, the residual stress will be locked in the specimens during the air cooling process. This will result in different mechanical properties for the specimens under annealing treatments, which motivates finding out the optimized annealing condition to remove the residual stress and thus efficiently stabilizing the mechanical property of solder.

The peak and onset of the melting temperatures are 183.3 and 181.1 °C for eutectic Sn–Pb alloy, respectively.[32] These critical temperatures were obtained by performing DSC (differential scanning calorimetry) scans for eutectic Sn–Pb samples, which were heated to 250 °C at a rate of 10 °C/min under the inert nitrogen atmosphere. The effect of annealing temperature was studied experimentally to remove the thermal residual stresses of polyphenylene sulphide by Wang et al.[33] They found that thermal residual stresses are relieved by annealing and the residual stress effect can be neglected at the temperature higher than 120 °C, denoted as a stress-free temperature (T_{SFT}) near its peak crystallization temperature. It means that above the T_{SFT}, slow cooling allows to remove the thermal residual stresses completely; otherwise, slow cooling below T_{SFT} can only partially remove these residual stresses. Compared with the annealing characteristics of semicrystalline polymeric matrix, the crystalline structure may show similar behavior. Therefore, the residual stress can be completely released if the annealing temperature is sufficiently close to melting temperature, even though there is no cold-crystallization temperature shown in the DSC curves of eutectic Sn–Pb material.[32] In the present study, the annealing condition is considered up to 180 °C, which is close to the melting temperature of the eutectic Sn–Pb alloy.

The testing program is listed in Table II considering practical annealing temperatures and durations. To assess the annealing effect on the tensile behavior of eutectic Sn–Pb alloy, low strain rates are preferred based on the intrinsic competition between creep and plasticity during

https://doi.org/10.1557/jmr.2017.166 Published online by Cambridge University Press

deformation. Based on some trial experiments for calibrating the reliability of testing conditions, three strain rates ranging from 10^{-4} s^{-1} to 10^{-3} s^{-1}, as listed in Table II, were chosen to achieve a balance between creep and plasticity and evaluate the theoretical modeling in Sec. III.

To objectively assess the annealing effect, four specimens were repeated for each annealing condition and strain rate. There were 120 specimens tested for different strain rates and annealing conditions. The stress–strain response provided in the present paper was obtained by averaging the response of repeated specimens subjected to the same preparation and test condition. It should be noted that compared with ultimate tensile strength, the facture strain of the specimens shows a greater randomness. Therefore, the provided tensile response was truncated when there was obvious declining due to the fracture of one specimen among the four repeated specimens. Therefore, the ductility in the present paper is conservative and may not be perfectly consistent with applied strain rates.

The dog-bone type specimens were carefully prepared with a high degree of uniformity. If no operation accident occurred during tensile tests, the measured complete stress–strain response was calibrated to be highly reliable. Despite of possible scatter in experimental data, the annealing effect on tensile behavior can still be revealed in terms of stress–strain response.

As shown in Table II, the annealing temperatures from 60 °C to 180 °C and the durations from 2 h to 48 h were chosen to investigate the effect of annealing and to find out the optimal annealing conditions. The chosen temperatures are corresponding to the homologous temperatures of 0.73 T_m, 0.82 T_m, 0.90 T_m and 0.99 T_m, respectively, where T_m = 456 K (i.e., 183 °C) is the melting temperature of the eutectic Sn–Pb solder. To optimize the deformation by avoiding premature localized damage, sufficient ductility, and stable ultimate tensile strength are accepted as the criterion of successful annealing treatment to release the local residual stress.

The 63Sn–37Pb bulk solder alloy was from Alpha Assembly Solutions (South Plainfield, New Jersey). The solder bars were manufactured using high purity raw materials to avoid impurities, while using viscosity and dross lowering treatment, the alloy was conditioned to be free of cast in impurities or included oxides. As listed in Table II, annealing was conducted for the machined specimens in an electric forced-air heating furnace so as to eliminate the residual work stress. During the heating process, it usually takes less than 0.5 h to elevate the furnace temperature from room temperature to the target temperature. By calibrating the temperatures on specimens, it was found that a certain difference existed between the set temperature and the reading from thermocouples attached on specimens due to the intrinsic limitation of forced-air heating approach. Thus, the reported temperatures in this paper are the corrected temperatures based on thermocouples.

TABLE II. Experimental analysis on the effects of annealing temperature, duration, and strain rate.

Annealing temperature (°C)	Annealing duration (h)	Strain rate (s^{-1})
60	2/6/12/24/48	5×10^{-4}
100	2/6/12/24/48	5×10^{-4}
140	2/6/12/24/48	5×10^{-4}
	2	$1 \times 10^{-3}/5 \times 10^{-4}/1 \times 10^{-4}$
	6	$1 \times 10^{-3}/5 \times 10^{-4}/1 \times 10^{-4}$
180	12	$1 \times 10^{-3}/5 \times 10^{-4}/1 \times 10^{-4}$
	24	$1 \times 10^{-3}/5 \times 10^{-4}/1 \times 10^{-4}$
	48	$1 \times 10^{-3}/5 \times 10^{-4}/1 \times 10^{-4}$

To investigate the tensile behavior of solder material, the dog-bone type specimen was designed in the present study by referring to the standard test methods provided by ASTM E8/E8M[34] for tension testing of metallic materials. It is regulated that the thickness should be between 0.1 and 3.0 mm, thus the geometrical details of specimen were correspondingly designed as proportional to the standard one, as shown in Fig. 1. It should be noted that the designed gauge length of 30 mm is greater than those reported by other researchers and the induced influence will be illustrated when analyzing the experimental results.

The uniaxial tensile tests were conducted in a manner of displacement controlled by using Bose ElectroForce 3330 mechanical test machine (TA Instruments, New Castle, Delaware). As the gauge length is about 30 mm as designed in Fig. 1, the applied velocity of clamps was calculated according to the respective strain rate. Considering that the Young's modulus of solder specimen is far less than that of clamp material, the tensile deformation of specimens were directly measured based on the recorded clamp movement. Thus, the strain during deformation was obtained by dividing the measured deformation by the gauge length of about 30 mm.

B. Control specimen without annealing treatment

The tensile tests were performed to the specimens machined from 63Sn–37Pb solder bars and stored at room temperature. No annealing conditions were provided for these specimens. The stress–strain relationships are tabulated in Table III to reflect the tensile behavior of solder material subjected to the strain rates of 1×10^{-3} s^{-1}, 5×10^{-4} s^{-1}, and 1×10^{-4} s^{-1}. The yielding initiation is defined by the 0.2% offset strain while the ultimate state before fracturing is considered as an obvious declining in measured stress–strain response. The yield strains of the tensile specimens vary in a negligible range due to the slight difference of elastic modulus, the annealing effect on yield strain is not discussed in

https://doi.org/10.1557/jmr.2017.166 Published online by Cambridge University Press

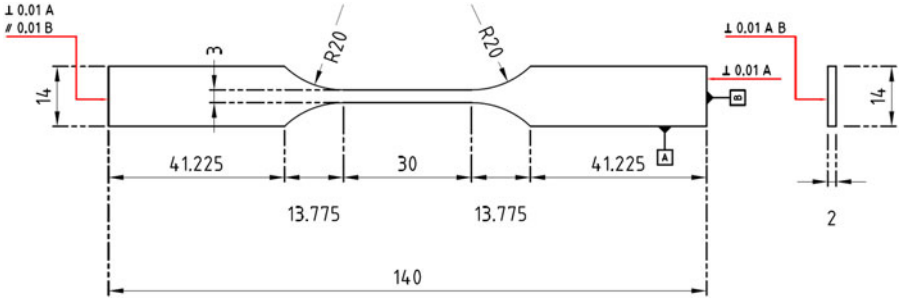


FIG. 1. Geometry of dog-bone type specimen made of bulk 63Sn–37Pb solder material (unit: mm).

TABLE III. Critical strain and stress of unannealed specimens subjected to different strain rates.

Strain rate (s^{-1})	Yield stress (MPa)	COV of yield stress	Ultimate strain (%)	Ultimate stress (MPa)	COV of ultimate stress
1×10^{-4}	29.45	0.07	9.41	34.20	0.09
5×10^{-4}	30.79	0.14	8.34	37.62	0.08
1×10^{-3}	37.56	0.03	7.77	41.69	0.08

Table III. To quantify the scatter information of experimental data, the coefficient of variation (COV) as a statistical measure of the distribution or dispersion of data around the average value is also provided in Table III.

It can be found that the ductility of unannealed specimens is less than 10% and too limited compared with the typical yielding and hardening behavior of solder alloys subjected to different strain rates. Thus, it is concluded that machined specimens of solder alloys without annealing treatment tends to be brittle. This abnormal phenomenon could be attributed to residual stress from the machining process. On the other hand, the micro defect (void/inclusion) in the prepared specimens may also increase the fracture contingency when the strain is not considered to be large. Hence, there is impediment for understanding the tensile properties of material, if there is no appropriate annealing process being made.

It is noteworthy that the ultimate tensile strain obtained in the present study is relatively less than the experimental results reported by other researchers. The underlying reason is that the gauge length in the present study is 30 mm, which is usually longer than those designed in the other studies. A similar gauge length of 25.4 mm was used by McDowell et al.[35] and the ultimate tensile stain of interest was about 0.05. It is well known that the plasticity of tested specimens is strongly influenced by dislocation/defect and could be localized at certain locations. Therefore, long gauge length could lead to the localized plasticity at multiple locations and one of the yielding locations will always fail much earlier than the others, which is confirmed by experimental observations in Fig. 2. On the other hand, the strain of tested specimens is

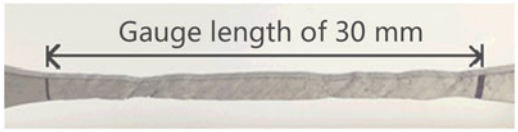


FIG. 2. Multiple yielding locations along the gauge length of 30 mm.

calculated by dividing the deformation measured from the clamped ends by the gauge length. Because the yielding/necking is negligible in most of the gauge length, the overall strain is much less when considering the deformation as the contribution of total gauge length.

C. Effect of annealing temperature

As shown in Table IV, some specimens failed due to tensile fracture within a strain less than 10%. This indicates that the annealing temperatures of 60 and 100 °C are insufficient to stably improve the ductility, even though the annealing duration up to 48 h was applied. As for 140 °C, the ultimate stresses after annealing of different durations are not consistent and cannot be accepted as a standard treatment. When the annealing temperature of 180 °C is applied, the tensile behavior of annealed specimens with increasing the annealing duration follows a certain trend and both of ductility and ultimate stresses are stabilized when the duration ranges from 6 h to 48 h. This duration range is possible to optimize the annealing condition. Therefore, the annealing temperature of 180 °C is ideal compared with other temperatures.

Higher annealing temperature results in more significant improvement of deformation capacity. As the strain increases, the defect-induced failure becomes more prone to initiate and propagate. Thus, it is reasonable to speculate that the higher annealing temperature effectively recovers the micro defects due to the casting and machining process of the specimens.

D. Effect of annealing duration

To examine the combined creep and plasticity deformation, three strain rates, 1×10^{-3} s^{-1}, 5×10^{-4} s^{-1},

https://doi.org/10.1557/jmr.2017.166 Published online by Cambridge University Press

and 1×10^{-4} s^{-1}, were applied to the specimens undergone the annealing temperature of 180 °C with the optimized deformation capacity. The critical stress and strain responses are summarized in Table V. Depending on the applied strain rate, both hardening and softening behavior can be observed for isothermally treated specimens at the same temperature and duration. However, besides annealing conditions, the ductility of annealed specimens was influenced by some other factors such as micro defects in form of void and inclusion that may initiate micro cracks and lead to final fracture when the overall deformation of specimen is not great, which is similar to the observations in Table II. Compared with tensile strength, the strain effect on ductility owns more randomness due to the inevitable micro defects in specimens.

TABLE IV. Critical strain and stress of specimens annealed at different temperatures under the strain rate of 5×10^{-4} s^{-1}.

Annealing temperature (°C)	Annealing duration (h)	Yield stress (MPa)	COV of yield stress	Ultimate strain (%)	Ultimate stress (MPa)	COV of ultimate stress
	2	34.88	0.04	9.48	40.33	0.02
	6	33.82	0.06	9.13	39.23	0.06
60	12	33.98	0.05	8.73	38.38	0.08
	24	32.24	0.18	11.01	40.40	0.10
	48	34.15	0.04	11.74	39.31	0.08
	2	33.15	0.16	9.85	42.46	0.08
	6	37.95	0.05	11.05	41.30	0.05
100	12	36.58	0.03	9.11	42.10	0.06
	24	39.12	0.02	9.19	44.29	0.03
	48	36.97	0.02	9.16	42.54	0.04
	2	43.24	0.06	11.29	50.12	0.07
	6	44.28	0.06	9.68	51.46	0.05
140	12	42.66	0.04	9.02	50.42	0.07
	24	40.71	0.12	10.57	48.61	0.06
	48	42.26	0.05	12.12	49.18	0.06
	2	47.95	0.06	12.79	54.45	0.05
	6	42.98	0.02	13.89	51.24	0.03
180	12	42.26	0.06	14.75	49.38	0.05
	24	41.25	0.04	16.05	48.75	0.03
	48	39.86	0.02	20.26	48.38	0.02

With the strain rate of 1×10^{-4} s^{-1}, the creep mechanism dominates the deformation and fracture with a limited deformation only occurs for the specimens annealed for 2 h. In terms of stress–strain relationship, the curve of the post-yielding stage is almost horizontal under the strain rate of 5×10^{-4} s^{-1}. This means the material response achieves a steady state and the stress maintains a constant value (usually defined as the saturation stress). Apparently, the saturation stress depends on both strain rate and annealing condition. Compared with other strain rates, the value of saturation stress of the specimens at the strain rate of 1×10^{-3} s^{-1} is higher. For each strain rate, longer annealing durations improve the ductility of specimens and stabilizes the ultimate tensile strength to a certain value. More importantly, material ductility is obviously improved when the annealing duration is increased from 2 h to 48 h.

On the other hand, the strain rate of 5×10^{-4} s^{-1} is appropriate to be the balance of creep and hardening deformation, which can be accepted as the strain rate to attain the saturation stress for the constitutive model proposed later. The strain rate of 5×10^{-4} s^{-1} is treated as the criterion of qualifying the annealing technique to release the residual stress and improve the ductility.

E. Optimization of the annealing condition

As shown in Table VI, compared with the tensile behavior of specimens without any annealing treatment at room temperature, the annealing temperature of 60 °C for

TABLE V. Critical strain and stress of specimens after different annealing durations at 180 °C.

Annealing duration (h)	Strain rate (s^{-1})	Yield stress (MPa)	COV of yield stress	Ultimate strain (%)	Ultimate stress (MPa)	COV of ultimate stress
	1×10^{-4}	39.66	0.10	6.25	45.00	0.09
2	5×10^{-4}	47.95	0.06	12.83	54.45	0.05
	1×10^{-3}	49.22	0.09	11.62	58.15	0.09
	1×10^{-4}	35.47	0.05	11.78	41.97	0.06
6	5×10^{-4}	42.98	0.02	13.72	51.24	0.03
	1×10^{-3}	45.53	0.05	15.08	55.02	0.04
	1×10^{-4}	31.74	0.15	16.95	39.68	0.07
12	5×10^{-4}	42.26	0.06	14.44	49.38	0.05
	1×10^{-3}	47.07	0.06	15.62	55.38	0.04
	1×10^{-4}	35.70	0.04	14.39	41.96	0.06
24	5×10^{-4}	41.25	0.04	15.81	48.75	0.03
	1×10^{-3}	45.16	0.04	14.08	54.79	0.02
	1×10^{-4}	36.84	0.06	17.38	40.53	0.04
48	5×10^{-4}	39.86	0.02	20.26	48.38	0.02
	1×10^{-3}	41.55	0.17	19.75	54.60	0.02

https://doi.org/10.1557/jmr.2017.166 Published online by Cambridge University Press

TABLE VI. Critical strain and stress of annealed specimens under the strain rate of 5×10^{-4} s^{-1}.

Annealing duration (h)	Annealing temperature (°C)	Yield stress (MPa)	COV of yield stress	Ultimate strain (%)	Ultimate stress (MPa)	COV of ultimate stress
	N/A	30.79	0.14	8.34	37.62	0.08
	60	34.88	0.04	9.48	40.33	0.02
2	100	33.15	0.16	9.85	42.46	0.08
	140	43.24	0.06	11.29	50.12	0.07
	180	47.95	0.06	12.79	54.45	0.05
	N/A	30.79	0.14	8.34	37.62	0.08
	60	33.82	0.06	9.13	39.23	0.06
6	100	37.95	0.05	11.05	41.30	0.05
	140	44.28	0.06	9.68	51.46	0.05
	180	42.98	0.02	13.89	51.24	0.03
	N/A	30.79	0.14	8.34	37.62	0.08
	60	33.98	0.05	8.73	38.38	0.08
12	100	36.58	0.03	9.11	42.10	0.06
	140	42.66	0.04	9.02	50.42	0.07
	180	42.26	0.06	14.75	49.38	0.05
	N/A	30.79	0.14	8.34	37.62	0.08
	60	32.24	0.18	11.01	40.40	0.10
24	100	39.12	0.02	9.19	44.29	0.03
	140	40.71	0.12	10.57	48.61	0.06
	180	41.25	0.04	16.05	48.75	0.03
	N/A	30.79	0.14	8.34	37.62	0.08
	60	34.15	0.04	11.74	39.31	0.08
48	100	36.97	0.02	9.16	42.54	0.04
	140	42.26	0.05	12.12	49.18	0.06
	180	39.86	0.02	20.26	48.38	0.02

2 h resulted in negligible effect on material ductility and ultimate tensile strength. With increasing annealing temperature, the ultimate tensile strength improved obviously from 60 °C to 140 °C, while the effect keeps insignificant between 140 and 180 °C. In terms of deformation capacity, the specimens behaved more ductile when the annealing temperature increased up to 180 °C. Therefore, to release the residual stress in the machined specimens, the annealing temperature should be greater than 100 °C if only 2 h of annealing duration is available. Similar phenomenon can be observed in the tensile behavior of specimens treated by 6 and 12 h, even though ultimate tensile strength is not improved from 140 °C to 180 °C.

When longer annealing treatment is provided, the general trend of ductility becomes irregular with the annealing durations of 24 and 48 h, while the ultimate tensile strength improves with the increasing annealing temperature. It should be noted that the annealing temperature 100 and 140 °C results in inconsistent effect for ultimate tensile strain, especially for the annealing durations greater than 12 h. Therefore, annealing more than 12 h is unnecessary and may lead to the overtreatment. On the other hand, the annealing temperature should be greater than 100 °C to release the residual stress and the duration should be less than 12 h to avoid inconsistent improvement of ductility.

In view of the overall effects of annealing condition on alloy mechanical properties, the optimal annealing treatment is determined as 180 °C for 6 h at a lower time cost to achieve improvement of both ductility and strength.

For the convenience of comparing the annealing effect at different temperatures and durations, the yield strength (YS), ultimate stress (US), and ultimate strain (USN) before fracturing in the stress–strain responses of all specimens are summarized with COVs in Fig. 3. The yielding initiation is simply defined by the 0.2% offset strain, while the final state before fracturing is considered as an obvious declining in measured stress–strain response. It should be noted that the effect of strain rate is explicitly accounted for in Figs. 3(a) and 3(c), while experimental results subjected to a constant strain rate of 5×10^{-4} s^{-1} are shown in Fig. 3(b). Compared with annealing duration, the annealing temperature generally owns more influence and higher temperature generally induces higher ultimate tensile stress and strain as shown in Figs. 3(a) and 3(b). As shown in the shadowed area of Fig. 3(a), the USN varies between 0.086 and 0.124 when annealing temperatures between 60 and 140 °C are applied for different durations. However, the annealing temperature of 180 °C induces significant ductility improvement in similar linear trends for different strain rates. On the other hand, both yield stress and ultimate stress gradually decay and become stabilized with increasing the annealing duration. So the annealing duration of 6 h is optimal due to a smaller COV as shown in the shadowed area of Fig. 3(b). Similar exponential decay is observed by assessing the critical stress-duration trends at different strain rates in Fig. 3(c). Based on extensive data comparisons above, mechanical property of specimens annealed at 180 °C for 6 h is acceptably stabilized with consistent improvement of both ductility and strength of solder alloy after machining process.

F. Annealing effect on rate dependence

The obtained ultimate tensile strengths are compared with the experimental data from Kawashima et al.,[21] Nose et al.,[22] and Shohji et al.,[23] as shown on Fig. 4. It is observed that the uniaxial tensile results in the current study (indicated by hollow symbols) agree well with the trend of tensile strength at different working temperatures, even though the applied strain rates of interest are not exactly the same. Meanwhile, the good correlation with other published experimental data support the evidence that despite only four specimens tested for each annealing condition and strain rate, the obtained stress–strain responses from the well prepared specimens in the present study are highly reliable. Thus, it is convincing that this annealing effect is not obtained randomly stemming from the scatter of experimental data.

For solder materials, the relationship between tensile strength σ and strain rate $\dot{\varepsilon}$ usually obeys the power law

https://doi.org/10.1557/jmr.2017.166 Published online by Cambridge University Press

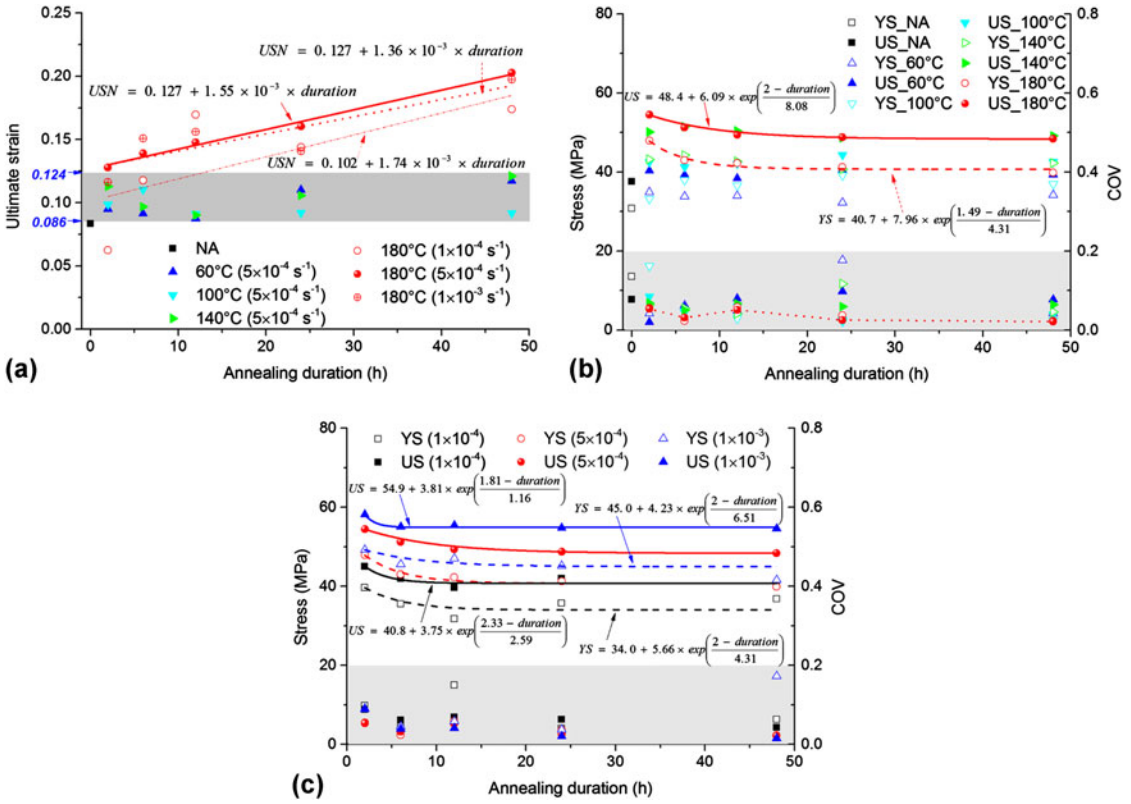


FIG. 3. Effect of annealing temperature and duration on critical strains and stresses: (a) ultimate strains subjected to different annealing temperatures and strain rates, (b) yield and ultimate stresses subjected to different annealing temperature and the constant strain rate of 5×10^{-4} s^{-1}, and (c) yield and ultimate stresses subjected to the annealing temperature of 180 °C and different strain rates.

$\sigma = B\dot{\varepsilon}^m$, where m is the strain rate sensitivity and B is a constant. The slope of $\log(\sigma)$ and $\log(\dot{\varepsilon})$ curve indicates the strain rate sensitivity of m. As shown in Fig. 4, the general slopes of the relationship between tensile strength and strain rate in the present experimental results are in good agreement with the other experimental data. It means that the strain rate sensitivity of the 63Sn–37Pb bulk solder studied herein is consistent with those from other experiments.[21–23] As for ultimate tensile strengths distribute along the stripe between −40 and 20 °C, this may attribute to the room temperature of 10 °C when storing and testing the annealed specimens in the present study.

By focusing on the relationship between tensile strength and strain rate of the present experimental study annealing at 180 °C, Fig. 5 shows that the ultimate tensile strengths of the cases with annealing for 2 h are obviously higher than those with longer annealing durations. Additionally, the distribution of the cases with annealing for 24 h is not of regular pattern and its slope is mostly different from the other annealing durations. Therefore, it is convincing to reconfirm the conclusion that 180 °C for 6 h is the optimal annealing treatment for Sn–Pb eutectic solder to well release the residual working stress in practice. As most of the COVs are less than 0.09, the consistency of data is satisfactory.

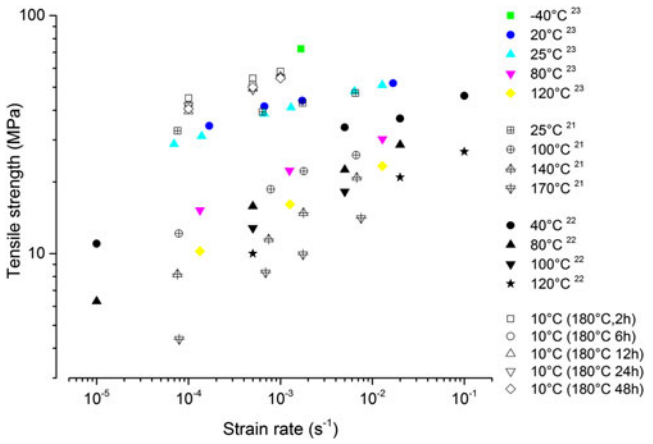


FIG. 4. Effect of strain rate and temperature on the tensile strength of 63Sn–37Pb solder.

III. A CONCISE UNIFIED CREEP AND PLASTICITY CONSTITUTIVE MODEL FOR SN–PB EUTECTIC SOLDER ALLOYS

Despite the observed impact of annealing condition is mainly with respect to ductility and strength, the mechanism dominating the rate dependent behavior remains to be elucidated. In the present study, a constitutive model is

https://doi.org/10.1557/jmr.2017.166 Published online by Cambridge University Press

proposed for Sn–Pb eutectic alloys with the parameters determined from the previous studies[36,37] and experimental data in the present work. To reveal the annealing effect, the experimental results under the annealing conditions at 180 °C for 2, 6, and 12 h are adopted in the numerical simulations.

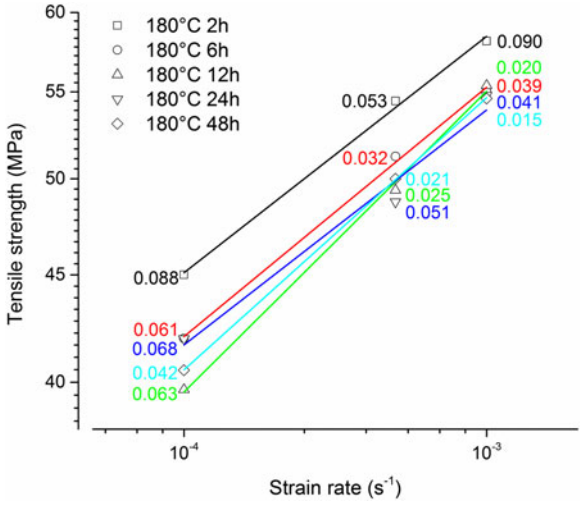


FIG. 5. Effect of annealing duration at 180 °C.

With the aim to exclusively investigate the effect of annealing condition to rate dependence, a concise constitutive model based on the unified creep and plasticity theory[36,37] is developed. The effects of the identical factors in the present experiments such as working temperature and damage evolution are ruling out, as shown in Eq. (1):

$$\dot{\varepsilon}^{\mathrm{in}} = A\left(\frac{s_{\mathrm{v}}}{d}\right)^{n}\mathbf{N} \quad . \tag{1}$$

The dominant parameters for the rate dependent behavior of 63Sn–37Pb solder is limited to the overstress s_{v} defined in Eq. (2), drag strength d defined in Eq. (3), and the flow direction N defined in Eq. (4) with the stress exponent n. Essentially, creep behavior and strain hardening effect of solder material are controlled by these parameters. The deviatoric stress tensor **S** is defined by Eq. (5).

$$s_{\mathrm{v}} = \left\langle \sqrt{\frac{3}{2}}\|\mathbf{S}\| - R \right\rangle \quad , \tag{2}$$

$$d = d_0 \mathrm{e}^{h\varepsilon_{\mathrm{eq}}^{\mathrm{in}}} \quad , \tag{3}$$

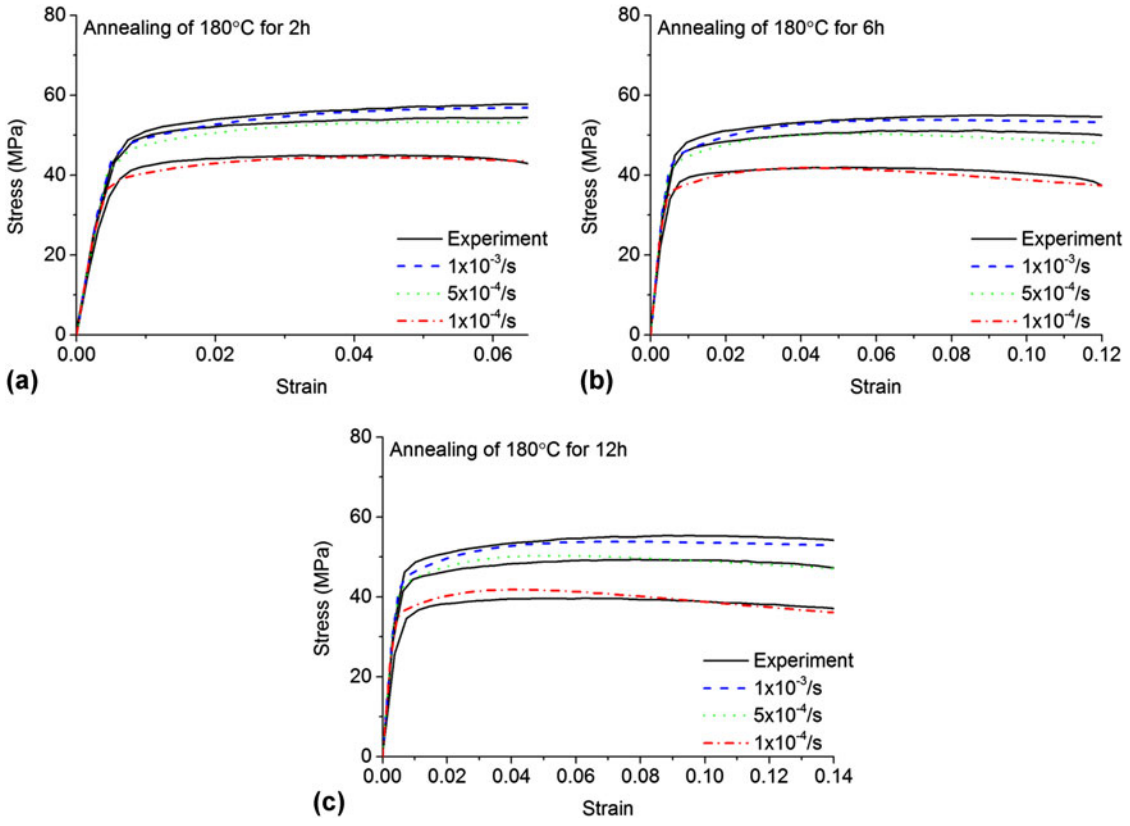


FIG. 6. Comparison of theoretical predictions by the proposed model and experimental results before the final failure of dog-bone type specimens annealed at (a) 180 °C for 2 h, (b) 180 °C for 6 h, and (c) 180 °C for 12 h.

https://doi.org/10.1557/jmr.2017.166 Published online by Cambridge University Press

$$\mathbf{N} = \mathbf{S}/\|\mathbf{S}\| \quad , \tag{4}$$

$$\mathbf{S} = \sigma - \frac{I_1}{3}\mathbf{I} \quad , \tag{5}$$

where I_1 is the first invariance of stress tensor $\boldsymbol{\sigma}$ defined as $\boldsymbol{\sigma}_{ii}$, $i = 1, 2, 3$ and $\mathbf{I}$ is a 3×3 identity matrix with the value of one on the main diagonal and zero elsewhere.

As the kinematic hardening of lead-rich solder is usually dominating the tensile behavior under cyclic loading scenarios,[37] the effect of kinematic hardening is neglected under monotonic tension in the present study. Thus, only the isotropic hardening is considered in this proposed model to control the center and radius of yield surface, as given in Eq. (6):

$$R = R_0 + (R_\infty - R_0)\left(1 - p\mathrm{e}^{-b\varepsilon_{\mathrm{eq}}^{\mathrm{in}}}\right) \quad , \tag{6}$$

where the accumulated inelastic equivalent strain $\varepsilon_{\mathrm{eq}}^{\mathrm{in}}$ from the start of analysis to the current time t is calculated in Eq. (7) by considering the contribution of inelastic strain at each time increment.

$$\varepsilon_{\mathrm{eq}}^{\mathrm{in}} = \int_0^t \frac{2}{3}\varepsilon_{ij}^{\mathrm{in}}\varepsilon_{ij}^{\mathrm{in}}\,\mathrm{d}\tau \quad . \tag{7}$$

The proposed model is programmed as a user-defined material (UMAT) subroutine in commercial finite element software ABAQUS.[38] The key inputs of the UMAT model are stress, strain, and solution-dependent state variables at the start of the current increment and also the increment of strain and time to reflect the strain rate of interest. After convergence, the UMAT model based on the proposed constitutive model can update and obtain the stress tensor at the end of each increment. The values of parameters are suggested as: $R_0 = 2$ MPa, $R_\infty = 20$ MPa, $d_0 = 20$ MPa, $b = 42$, and $P = 0.8$ for Sn–Pb eutectic alloy. As observed in Fig. 6, the proposed model is capable of accurately predicting stress–strain responses and the strain rate of 5×10^{-4} s^{-1} could be a suitable experimental loading rate to investigate the saturation stress with a sufficient stress plateau, at which the creep and plasticity mechanism counteract each other. The parameters A, h, and n provided in Fig. 7 are determined by numerical regression to the tensile behavior before the final failure of the tested dog-bone type specimens. To illustrate the correlation between strain rate and these

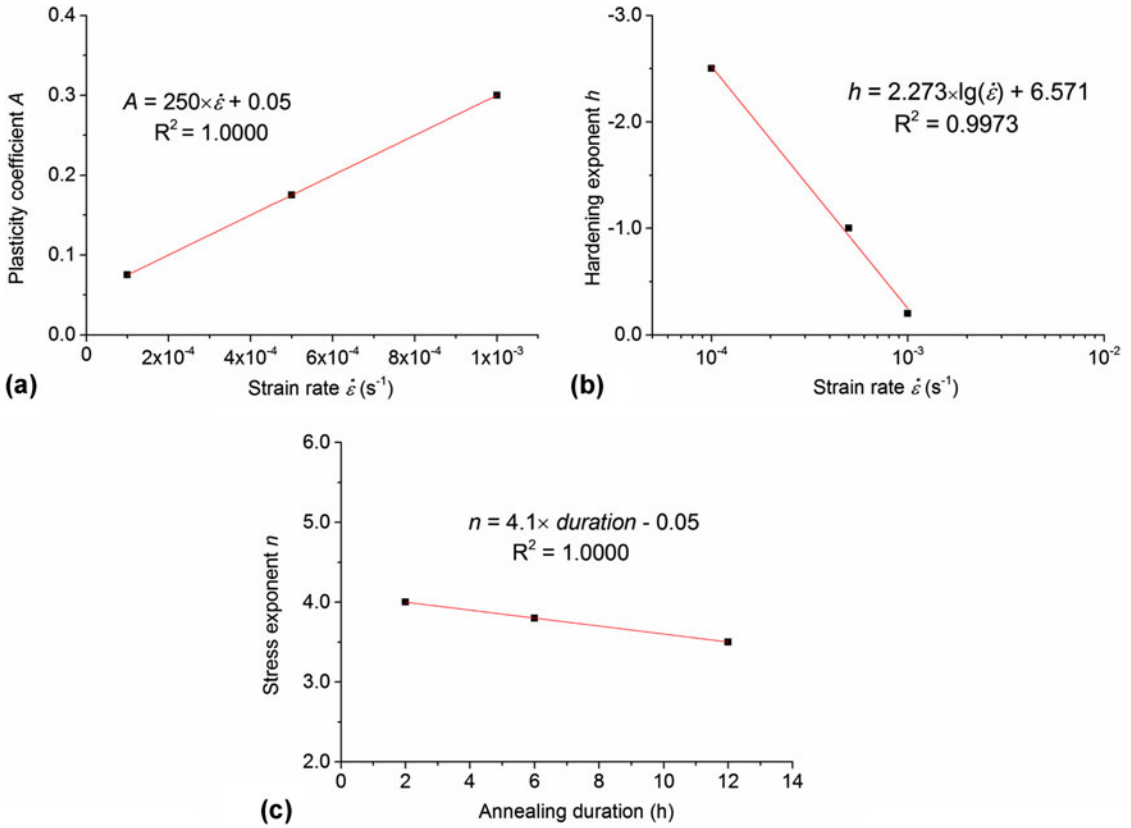


FIG. 7. Parameter calibration of the proposed constitutive model: (a) rate dependence of plasticity coefficient A, (b) rate dependence of hardening coefficient h, (c) effect of annealing duration on the stress exponent n at 180 °C.

https://doi.org/10.1557/jmr.2017.166 Published online by Cambridge University Press

parameters, the statistical relationship between actual and curved-fitted values is described by the coefficient of determination, denoted as R^2, which is used to quantify how well the regression line predicts the actual data. As shown in Figs. 7(a) and 7(b), the parameters of plasticity coefficient A and hardening coefficient h are found to be rate dependent. Meanwhile, Fig. 7(c) shows the annealing effect on rate dependence of Sn–Pb eutectic alloys. With a gentle negative slope, the stress exponent n linearly decays with increasing of the annealing duration at 180 °C. Thus, the annealing duration of 6 h at 180 °C is able to attain a stable rate dependent property of the Sn–Pb eutectic solder, which coincides with the conclusion of optimized annealing condition from experimental observations. Furthermore, all parameters in the proposed model are well linearly dependent on the applied strain rate or annealing duration. This means these parameters have clear physical meanings with respect to plasticity and hardening.

IV. CONCLUSIONS

The effect of annealing condition including temperature and duration was investigated experimentally and theoretically for Sn–Pb eutectic solder alloy under strain rates from 10^{-4} s^{-1} to 10^{-3} s^{-1}. With the temperatures ranging from 60 °C to 180 °C and durations from 2 h to 48 h, it was experimentally observed that the optimal annealing condition is 180 °C for 6 h to well release the residual stress in the dog-bone type specimens, and a consistent improvement of tensile properties is achieved in terms of ultimate strength and ductility. The relationships between tensile strength and strain rate from the current experimental results agreed with others from literature. With a balance of creep and hardening mechanism, the strain rate of 5×10^{-4} s^{-1} can be treated as a suitable experimental loading rate to investigate the saturation stress of 63Sn–37Pb solder alloy with a sufficient and stable plateau. By proposing a concise constitutive model based on the unified creep and plasticity theory, the dominant parameters with clear physical meanings were determined by regression to the tensile behavior of the tested specimens. The values of plasticity coefficient A, hardening coefficient h, and stress exponent n are linearly dependent to the applied strain rates with a sufficiently satisfactory correlation. Similar to the optimization of annealing condition based on experimental studies, the annealing duration of 6 h at 180 °C is found to be able to attain a stable rate dependent property of the Sn–Pb eutectic solder alloy. To improve the mechanical performance consistently, the annealing duration of 6 h at 180 °C is ascertained to be the optimized annealing condition.

After annealing treatment, the residual state including microstructure in the specimens is important to reveal the material intrinsic property from the material science point of view. The authors are actively considering the nanoindentation method to examine the residual stress in the annealed specimens in the near future to confirm the optimized annealing condition for solder materials.

It should be noted that the proposed annealing condition of this study is only applicable to Sn–Pb eutectic solder specimen machined from solder bars and stored at room temperature. The optimized annealing conditions for lead-free solders such as Sn–3.0Ag–0.5Cu can be similarly investigated by performing constitutive experiments referring to their melting temperatures.

ACKNOWLEDGMENTS

The authors are grateful for the supports provided by National Natural Science Foundation of China (51508464, 11572249). This work was also partially supported by "the Fundamental Research Funds for the Central Universities" (No. 3102016ZY017).

REFERENCES

1. M. Osterman: Being "RoHS Exempt" in a Pb-free world. Presented at the *Capital SMTA Chapter Pb-free Tutorial Program* (Electronic Products and Systems Center, Maryland, 2006).
2. Directive EU: European Parliament legislative resolution of 24 November 2010 on the proposal for a directive of the European Parliament and of the Council on the restriction of the use of certain hazardous substances in electrical and electronic equipment A7–0196/2010 (2010).
3. I.C. Turner, B.D. Dunn, and C. Barnes: A study into the reprocessing of pure tin termination finishes into tin–lead. *Soldering Surf. Mt. Tech.* **25**(4), 218 (2013).
4. B.D. Dunn and G. Mozdzen: Tin oxide coverage on tin whisker surfaces, measurements and implications for electronic circuits. *Soldering Surf. Mt. Tech.* **26**(3), 139 (2014).
5. ECSS-Q-ST-70–08C: *Space Product Assurance: The Manual Soldering of High-reliability Electrical Connections* (European Cooperation for Space Standardization, Noordwijk, 2009).
6. ECSS-Q-ST-70–38C: *Space Product Assurance, High-reliability Soldering for Surface-mount and Mixed Technology* (European Cooperation for Space Standardization, Noordwijk, 2008).
7. A. Rusinko: Modeling the effect of DC on the creep of metals in terms of the synthetic theory of irrecoverable deformation. *Mech. Mater.* **93**, 163 (2016).
8. G. Chen and X. Chen: Fatigue damage coupled constitutive model for 63Sn37Pb solder under proportional and non-proportional loading. *Mech. Mater.* **39**(1), 11 (2007).
9. M. Mustafa, J.C. Suhling, and P. Lall: Experimental determination of fatigue behavior of lead free solder joints in microelectronic packaging subjected to isothermal aging. *Microelectron. Reliab.* **56**, 136 (2015).
10. F. Ochoa, J.J. Williams, and N. Chawla: Effects of cooling rate on the microstructure and tensile behavior of a Sn–3.5 wt% Ag solder. *J. Electron. Mater.* **32**(32), 1414 (2003).
11. X. Hu, W. Chen, X. Yu, Y. Li, Y. Liu, and Z. Min: Shear strengths and fracture behaviors of Cu/Sn37Pb/Cu soldered joints subjected to different displacement rates. *J. Alloys Compd.* **600**, 13 (2014).
12. K.S. Kim, S.H. Huh, and K. Suganuma: Effects of cooling speed on microstructure and tensile properties of Sn–Ag–Cu alloys. *Mater. Sci. Eng., A* **333**(1–2), 106 (2002).

https://doi.org/10.1557/jmr.2017.166 Published online by Cambridge University Press

13. P. Vianco, J. Rejent, G. Zender, and A. Kilgo: Kinetics of Pb-rich phase particle coarsening in Sn–Pb solder under isothermal annealing–cooling rate dependence. *J. Mater. Res.* **20**(6), 1563 (2005).
14. T.Y. Lee, W.J. Choi, K.N. Tu, J.W. Jang, S.M. Kuo, J.K. Lin, D.R. Frear, K. Zeng, and J.K. Kivilahti: Morphology, kinetics, and thermodynamics of solid-state aging of eutectic SnPb and Pb-free solders (Sn–3.5Ag, Sn–3.8Ag–0.7Cu and Sn–0.7Cu) on Cu. *J. Mater. Res.* **17**(2), 291 (2002).
15. K.I. Ohguchi and K. Kurosawa: An evaluation method for tensile characteristics of Cu/Sn IMCs using miniature composite solder specimen. *J. Electron. Mater.* **45**(6), 3183 (2016).
16. C.M. Chuang, T.S. Lui, and L.H. Chen: Effect of lead content on vibration fracture behavior of Pb–Sn eutectic solder. *J. Mater. Res.* **16**(9), 2644 (2001).
17. K. Jung and H. Conrad: Microstructure coarsening during static annealing of 60Sn40Pb solder joints: I stereology. *J. Electron. Mater.* **30**(10), 1294 (2001).
18. L.N. Ramanathan, J.W. Jang, J.K. Lin, and D.R. Frear: Solid-state annealing behavior of two high-Pb solders, 95Pb5Sn and 90Pb10Sn, on Cu under bump metallurgy. *J. Electron. Mater.* **34**(10), L43 (2005).
19. J-W. Jang, A.P. De Silva, J-K. Lin, and D.R. Frear: Tensile fracture behaviors of solid-state-annealed eutectic SnPb and lead-free solder flip chip bumps. *J. Mater. Res.* **19**(6), 1826 (2004).
20. Y. Xu, S. Ou, K.N. Tu, K. Zeng, and R. Dunne: Measurement of impact toughness of eutectic SnPb and SnAgCu solder joints in ball grid array by mini-impact tester. *J. Mater. Res.* **23**(5), 1482 (2008).
21. K. Kawashima, T. Ito, and M. Sakuragi: Strain-rate and temperature-dependent stress–strain curves of Sn–Pb eutectic alloy. *J. Mater. Sci.* **27**(23), 6387 (1992).
22. H. Nose, M. Sakane, Y. Tsukada, and H. Nishimura: Temperature and strain rate effects on tensile strength and inelastic constitutive relationship of Sn–Pb solders. *J. Electron. Packag.* **125**(1), 59 (2003).
23. I. Shohji, T. Yoshida, T. Takahashi, and S. Hioki: Comparison of low-melting lead-free solders in tensile properties with Sn–Pb eutectic solder. *J. Mater. Sci.: Mater. Electron.* **15**(4), 219 (2004).
24. I. Shohji, T. Yoshida, T. Takahashi, and S. Hioki: Tensile properties of Sn–Ag based lead-free solders and strain rate sensitivity. *Mater. Sci. Eng., A* **366**(1), 50 (2004).
25. L. Zhang, X. Chen, H. Nose, and M. Sakane: Stress–strain behaviors of 63Sn37Pb solder simulated by anand model. *J. Mech. Strength* **26**(4), 447 (2004).
26. X. Chen, D. Jin, M. Sakane, and T. Yamamoto: Multiaxial low-cycle fatigue of 63Sn–37Pb solder. *J. Electron. Mater.* **34**(1), L1 (2005).
27. R. Chen and F. Yang: Electrocontact heating in a Sn60Pb40 solder alloy. *J. Phys. D: Appl. Phys.* **41**(41), 3142 (2008).
28. R. Chen and F. Yang: Impression creep of a Sn60Pb40 alloy: The effect of electric current. *J. Phys. D: Appl. Phys.* **41**(15), 1525 (2008).
29. F.Z. Xuan, S.S. Shao, and Q.Q. Chen: Synthesis creep behavior of Sn63Pb37 under the applied stress and electric current. *Microelectron. Reliab.* **51**(12), 2336 (2011).
30. T. Hurtony, A. Szakál, L. Almásy, A. Len, S. Kugler, A. Bonyár, and P. Gordon: Characterization of the microstructure of tin–silver lead free solder. *J. Alloys Compd.* **672**, 13 (2016).
31. W. Yang, L.E. Felton, and R.W. Messler: The effect of soldering process variables on the microstructure and mechanical properties of eutectic Sn–Ag/Cu solder joints. *J. Electron. Mater.* **24**(10), 1465 (1995).
32. K.M. Kumar, V. Kripesh, and A.A.O. Tay: Influence of single-wall carbon nanotube addition on the microstructural and tensile properties of Sn–Pb solder alloy. *J. Alloys Compd.* **455**(1–2), 148 (2008).
33. X. Wang, D. Xu, H. Liu, H. Zhou, Y. Mai, J. Yang, and E. Li: Effects of thermal residual stress on interfacial properties of polyphenylene sulphide/carbon fibre (PPS/CF) composite by microbond test. *J. Mater. Sci.* **51**(1), 334 (2016).
34. Annual Book of ASTM Standards: *Standard Test Methods for Tension Testing of Metallic Materials* (American Association State, Pennsylvania, 2009).
35. D.L. McDowell, M.P. Miller, and D.C. Brooks: A unified creep-plasticity theory for solder alloys. In *Fatigue of Electronic Materials*. (ASTM International, Philadelphia, 1994).
36. Y. Yao, L.M. Keer, and M.E. Fine: Modeling the failure of intermetallic/solder interfaces. *Intermetallics* **18**(8), 1603 (2010).
37. Y. Yao, H. Xu, L.M. Keer, and M.E. Fine: A continuum damage mechanics-based unified creep and plasticity model for solder materials. *Acta Mater.* **83**, 160 (2015).
38. Dassault Systemes Simulia Corp.: *ABAQUS 6.14–4* (Hibbitt, Karlsson & Sorensen, Rhode Island, 2014).

https://doi.org/10.1557/jmr.2017.166 Published online by Cambridge University Press